Monatsh Chem (2010) 141:1279–1285
DOI 10.1007/s00706-010-0401-6

ORIGINAL PAPER

Research on the rupture of the covalent bond of the dichlorine molecule

Dongfang Zhang

Received: 23 April 2010 / Accepted: 11 September 2010 / Published online: 20 October 2010

Abstract Photoinduced reaction of gas-phase dichlorine molecules on the short wavelength side of the A-band gives a negative value for the asymmetry parameter of Cl ($^2P_{1/2}$) fragments, which conflicts with the intrinsic electronic transition mechanism. In this paper, the dissociation process of the dichlorine molecule has been investigated at numerous excitation wavelengths in the range 310–470 nm using the numerical method and the frontier molecular orbital maps are drawn to obtain insight into the character of the relevant molecular orbitals. The possibilities of radial nonadiabatic transition from the $C^1\Pi_u$ to the third $\Omega = 1_u$ ($\sigma_u^* \leftarrow \sigma_g$) electronic state are also examined, and found to cause large variations for the angular distribution functions. The wavelength dependence of the beta parameter β_2(Cl*), which is computed from the partial cross-section with the RZD transition mechanism, agrees with the experimental behavior and further justifies the conclusion that the decrease of beta in the Cl + Cl* channel is because of the radial nonadiabatic interaction between the C and 1_u(III) excited states and this interaction is a key mechanism decreasing the beta parameter value. At last, the kinetic energy distributions of fragments are obtained in the asymptotic region.

Keywords Photochemistry · Electronic excitation · Nonadiabatic transition

D. Zhang (✉)
College of Science, Huazhong Agricultural University, Wuhan 430070, People's Republic of China
e-mail: zjzappletree@126.com

Introduction

Nowadays, the importance of nonadiabatic phenomena in photochemical processes can hardly be overestimated. In a sense, the Born–Oppenheimer approximation (which assumes that electrons can quickly accommodate to any movement of nuclei) leads to calculations of the propagation of nuclei, quantum–mechanically, classically, or semiclassically, on computed electron surfaces. These potential surfaces may be obtained either from highly accurate, but demanding electronic structure calculations or from appropriate parameterizations [1]. In the former case, the required number of quantum chemical calculations can be very large and complex depending on the size of the system [2]. Therefore, "on-the-fly" approaches to the dynamics of nuclei and electrons have recently become popular, leading to the sub-field of ab-initio molecular dynamics [3]. If the nuclei are treated classically, the forces on the nuclei can be regarded as electronic glue holding a molecule together. This approach, when combined with full quantum or semiclassical dynamics schemes, has the potential to treat large problems accurately with the complete machinery of quantum dynamics [4]. However, when two and more potential surfaces undergo avoided crossings, much more sophisticated quantum treatment is needed to track the bifurcation of quantum wavepackets which results in the so-called entangled state between electrons and nuclei through nonadiabatic transition (i.e., nuclear-wavepacket bifurcation due to nonadiabatic transition) [5]. In fact, many theories have been devoted to nonadiabatic transitions, most of which are extensions and generalizations of the semiclassical theory, for example the Landau–Zener–Stuekelberg approach [6], the mean-field or surface hopping models [7], and one-dimensionally reduced full quantum calculations [8].

The photodissociation of dihalogen molecules (Br_2, I_2, etc.) has been extensively studied for decades, because of the effects of their photodissociation products on ozone depletion and the fundamental interest in photodissociation dynamics [9, 10]. In particular, the dihalogen molecule, for example Cl_2, has attracted much attention as an etalon system in research on the photodissociation process [11–13]. The well-known first absorption band of the Cl_2 molecule is located in the UV region with a maximum at ~330 nm and corresponds to molecular excitation to the valence states correlating with the $Cl(^2P_J,\ J = 1/2,\ 3/2)$ atomic products. Roughly speaking, there are three possible dissociation channels corresponding to different combinations of the Cl atoms in their spin-excited $Cl^*(^2P_{1/2})$ and ground $Cl(^2P_{3/2})$ states. The B state correlates with excited state chlorine atoms in the adiabatic approximation, whereas the C and A states yield ground-state Cl atoms upon dissociation. Despite extensive investigations of the Cl_2 photodissociation in the first absorption band [14–19], information about the dissociation pathway and nonadiabatic interplay between the relevant excited states is still not complete and unambiguous. The nonadiabatic transition can also affect the photodissociation process and it becomes more complex as the photolysis energy increases [20, 21]. According to previous studies, it is concluded that 12% dissociate via the parallel (B) state whereas 88% dissociate via the perpendicular (C) state. From the value of beta measured at 330 nm, however, the C state correlates adiabatically to Cl + Cl, so the question which must be solved is, what electronic states of Cl_2 are involved and in which direction do the $Cl^*(^2P_{1/2})$ fragments go? Because the effects of interference on the orientation of the total angular momentum of the products are quite sensitive to the details of the entire photodissociation processes, their theoretical simulation would provide important information about the dissociation dynamics and tell if the Cl atoms jumped state during dissociation.

In this study, we explore the photodissociation dynamics of Cl_2 and examine the nonadiabatic transition processes that cause branching or angular distribution of the products. Moreover, the kinetic energy distributions of fragments are obtained by undertaking a long-term propagation scheme to obtain information about wavepacket evolution. Starting from multi-configurational SCF computations of the excited state potential energy states and following these with wavepacket calculations of the photodissociation dynamics, the problem of theoretical description of photofragment angular distribution from photolysis of Cl_2 molecules via the first absorption band was addressed with possible nonadiabatic interactions being taken into account. It will become clear that the contribution of the radial nonadiabatic transition is dominant, whereas that of the rotational nonadiabatic transition is negligibly small. This radial nonadiabatic transition is considered to follow the RZD model. Based on these results on the scattering calculations, the radial kinetic energy operator or the L-uncoupling operator-induced coupling mechanism that promotes nonadiabatic transfer is analyzed to explain quantum-mechanical interference effects in the fragmentation process.

Results and discussion

Molecular constants and electronic structures

The one-dimensional potential surfaces of Cl_2 are plotted in Fig. 1, which corresponds to the change of the potential energy values versus the Cl–Cl bond length as a geometric property. These computed potential energy curves for the ground and excited valence Cl_2 states will be exploited to execute the time-dependent wave packet calculations. First, the ground state vibrational wave functions are obtained by numerical solution of the one-dimensional nuclear Schrödinger equation, in which the ground state potential (interpolated with smooth cubic spline) is used. The excited state potentials are then used in the wave packet evolution; the ground state potential is irrelevant for calculations of the excited state dynamics once the initial wave packets are generated. The interaction potentials, adopted in the wavepacket calculations, have a correct long-range character, proportional to R^{-6}. To estimate accuracy of the computed potential energy curves and the quality of the further calculations based on these potentials, a comparison has been made between calculation and experiment for the molecular constants of the $X^1\Sigma_g^+$, $A^3\Pi_{1u}$, and $B^3\Pi_{0+u}$ states of Cl_2; the results are shown in Table 1. Because the

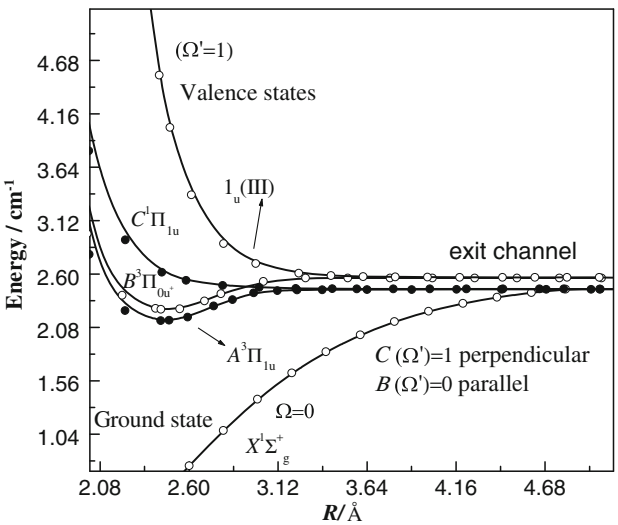

Fig. 1 One-dimensional potential cuts along the stretching coordinate R of molecular chlorine. The limit $E = 0$ corresponds to two separated atoms

Table 1 Characteristic data of the potential energy surfaces important for the photodissociation of molecular chlorine from visible to near UV

State	R_0 (a_0)	D_0 (eV)	ω_0 (cm^{-1})	$\omega_0 x_0$ (cm^{-1})
$X^1\Sigma_g^+$				
Calc.	3.860	2.396	539.04	3.69
Expt.	3.758	2.475	559.70	2.67
$A^3\Pi_{1u}$				
Calc.	4.605	0.308	277.9	7.27
Expt.	4.601	0.313	265.0	5.0
$B^3\Pi_{0+u}$				
Calc.	4.609	0.310	273.1	7.71
Expt.	4.605	0.380	259.5	5.3

D_0 equilibrium dissociation energy, R_0 equilibrium bond length, ω_0 vibrational frequencies, $\omega_0 x_0$, anharmonic constants

$C^1\Pi_{1u}$ and 1_u(III) states are all repulsive in the Franck–Condon and asymptotic region, no spectroscopic constants can be obtained for them. Thus, no comparison with experiment is possible in this case. The computed data for the electronic states is in good agreement with the experimental results [22]. For example, the $X^1\Sigma_g^+$ equilibrium bond distance is slightly overestimated (by $\sim$0.102 a_0), whereas the corresponding vibrational frequency ω_0 is too low by 20.66 cm^{-1}. Thus, it is expected that quantitative results can be obtained for the photodissociation processes with these ab-initio potential energy curves. In addition, one can note that the accuracy of the ground state potential in the Franck–Condon region is notably better than the bonding strength value, which should enable fairly reliable calculation of the absorption spectrum. It is worth noting that the spin–orbital interaction has no significant effect on the ground state dissociation energy.

In order to better understand the dynamics present in the photolysis processes, we carried out time-dependent density-functional theory (TD-DFT) calculations and the molecular orbitals (MOs) were plotted by using the Chemview suite of programs. Figure 2 shows the character of the relevant orbitals involved in the electronic configuration, which are calculated using the TD-BHandHLYP/6-31G* method in the gas phase, although TD-DFT may underestimate the long-range Coulomb interactions in charge-transfer excited states in an overall neutral molecule. Fortunately, the use of increased HF exchange (50% in BHandHLYP) is found to give a good description of the charge-transfer excited state. The MOs considered here are those that are relevant in Cl–Cl cleavage of the Cl_2 molecule. Apparently, in the picture, the lone-pair orbital of the atoms, which are the five energetically highest occupied MOs, become the main source for the formation of the low-lying excited states. According to the computations, in both states the transition from HOMO to LUMO (14a $\rightarrow$ 19a) calculated at 14.43 eV (85.91 nm) and transition (17, 18a $\rightarrow$ 19a) calculated at 3.785 eV (327.56 nm) are found to dominate the absorption from the estimated oscillator strength $f = 0.0024$ and $f = 0.0858$. Because the excitation energies for the 14a $\rightarrow$ 19a transition lie very close to the Rydberg transition, and the absorption spectrum band can be ascribed largely to the transitions to the first lowest unoccupied molecular orbital, namely, the front virtual orbital, the photon energy required for excitation is approximately 3.785 eV (327.56 nm) and transition to the $C^1\Pi_1$ state can be achieved. This indicates that the absorption profile will show a maximum coefficient near the wavelength of 330 nm. In addition, the 1_u(III) $\leftarrow$ X transition moment is rather weak ($\ll$0.025 ea_0) in terms of the Franck–Condon envelope and photoexcitation to the 1_u(III) state requires much more energy in the Franck–Condon region. So the initial vertical excitation to the 1_u(III) state can be practically disregarded because no direct transitions to the triplet $^3\Sigma^+$ components can occur.

Use of the Rozen–Zener–Demkov (RZD)-type transition

If the system has a clear avoided crossing as a function of the adiabatic parameter and the radial transition between adiabatic states with the same symmetry is expected to play an important role in branching phenomena, the RZD type transition can be used. For Cl_2 photodissociation, two types of non-adiabatic transition, which partly occur from the second $\Omega = 1_u$ (C) state to states dissociating into Cl + Cl* should be considered:

1. heterogeneous transition ($\Delta\Omega = 1$), occurring between the $B^3\Pi_{0+u}$ and $C^1\Pi_u$ states with different symmetry, which intersect each other on their pathways to dissociation; and
2. homogenous transition ($\Delta\Omega = 0$), induced by the coupling between the states of the same 1_u symmetry.

The heterogeneous transition comes from Coriolis coupling, which depends on the rotational temperature, and the rotational period is usually very small. The homogenous transition is caused by radial derivative coupling, which means non-adiabatic transition from the C to the 1_u(III) state may take place because of the small spin–orbit splitting, and the factor is found to be dominant. For these reasons, the radial coupling between the C and 1_u(III) states is considered in our calculations, in which the non-crossing RZD model is used. For applicability of the RZD model, the two involved diabatic states (C and 1_u(III)) are labeled as letters *i* and *j*, and wave functions for the coupled states are denoted φ_i and φ_j. In the asymptotic region, because the distance between the two chlorine atoms is large and the coulombic force is rather weak, the coupling mode of the two atomic wave functions can be treated within a

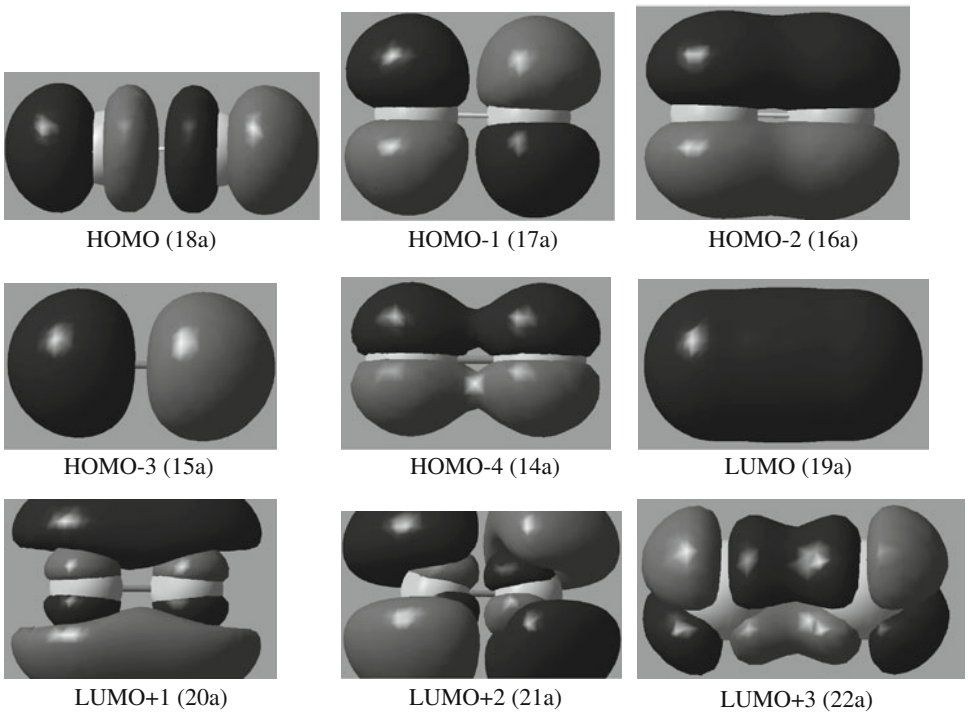

Fig. 2 Profiles of the frontier MOs that participate in the course of dissociation, which correlate with the low-lying excited states of Cl_2

Jj-coupling scheme. By this description, the energy spacing between diabatic potential curves in the asymptotic region can be defined as $\Delta = H_{jj} - H_{ii}$, which reveals weak dependence on the internuclear distance R and corresponds to the spin–orbit splitting of chlorine atoms, especially at longer R. Their coupling matrix element H_{ij} corresponds to exchange interaction caused by the coulombic force between the two chlorine atoms, and H_{ij} is supposed to be an exponential type as $H_{ij} = A{\cdot}\exp(-\alpha R)$. In this case, H_{ij} will diminish exponentially with bond distance R in the dissociation regions and the exchange interaction is less important at a long-range distance.

The Hamiltonian of the RZD model in the diabatic representation is given by:

$$H_{RZ} = \begin{bmatrix} \Delta/2 & A\exp(\gamma t) \\ A\exp(\gamma t) & -\Delta/2 \end{bmatrix} \quad (1)$$

This model describes the process in the case of coupling of the electronic wave functions. The nonadiabatic transition occurs at $t = \log(\Delta/A)/\gamma$, and the transition probability p is given by:

$$p = \frac{1}{1 + \exp(2\delta)} \quad (2)$$

where $\delta = \pi\Delta/2\hbar\gamma$. An extreme value of $\alpha/4$ occurs at $R = R_0$, where $A{*}\exp(-\alpha R_0) = \Delta/2$ is satisfied. If R is small, the relative position of the nucleus is near the Franck–Condon region and electrostatic force is responsible for the dominant interaction, because $H_{ij} \gg \Delta$, wave functions of the two states are governed by ΛS-coupling. However, with increasing interatomic distance in Cl_2, couplings among the electronic states become more comparable in magnitude with the differences between the potential energies of these states. As R exceeds a threshold R_0, the exchange interaction and spin–orbit interaction have equal magnitude and recoupling of the adiabatic wave functions happens, which induces non-adiabatic transition from C to the higher 1_u(III) state.

The energy gap of the coupled states i and j would behave as:

$$E_{1u} - E_C = \left[\Delta^2 + 4A^2\exp(-2\alpha R)\right]^{1/2} \quad (3)$$

α, A, and Δ are obtained by fitting Eq. (3) with ab-initio data. The final results are $R_0 = 6.57$ a_0, $\Delta = 0.004$ hartree, $\alpha = 1.128(a_0^{-1})$, and $A = 6.679$ hartree. It follows from the Eq. (2) that as υ becomes larger with higher photon energy, p increases as the excitation wavelength becomes shorter.

Modeling of the angular distribution function

In general, the photodissociation dynamics for Cl_2 are simple and only correlate with the prompt dissociation channel originating from the Cl–Cl stretching mode, while two independent reaction paths on the excited potential energy surfaces are found. The Cl_2 molecule dissociates through two kinds of transitions after absorbing a single photon. $1_u \leftarrow 0_g^+$ is attributed to a perpendicular transition ($\Delta\Omega = 1$) and $0_u^+ \leftarrow 0_g^+$ ($X^1\Sigma_g$) constitutes a parallel transition ($\Delta\Omega = 0$). The angular distribution of fragments is represented as $f(\theta) \propto 1 + \beta_2{\cdot}P_2(\cos\theta) + \beta_4{\cdot}P_4(\cos\theta)$,

where β_2 is the asymmetry parameter contributing to the angular distribution, because the orientation is described by the odd ranks $K = 1, 3$ and, therefore, this effect does not contribute to the angular distribution given in the above formula. The term proportional to β_4 usually appears because of the alignment of the photofragment angular momentum or because of initial asymmetry of the parent molecular axis. However, the alignment effect is small, because the molecules have axial symmetry and recoil fast along the bond direction, and thus the term containing β_4 vanishes from the above formula. For prompt dissociation $\beta_2 = 2$ if transition is parallel and $\beta_2 = -1$ if a perpendicular transition is involved. The dynamic calculations only take account of the initial wave packets created on the A, B, and C state potentials. From the adiabatic correlation of Cl_2 and the prediction of radial non-adiabatic transition, it can be seen that the Cl* fragments may have dual sources, the B state (directly) and C state (indirectly). The latter is devoted to Cl* production via the 1_u(III) state, which adiabatically correlates with the Cl +Cl*. The angular distribution function β_2(Cl*) can be calculated by implementing the RZD model mentioned earlier with the assumption of the axial recoil approximation:

$$\beta_2 = \frac{-\varepsilon(\mathrm{C} \leftarrow \mathrm{X}) \cdot p + 2\varepsilon(\mathrm{B} \leftarrow \mathrm{X})}{\varepsilon(\mathrm{C} \leftarrow \mathrm{X}) \cdot tp + \varepsilon((\mathrm{B} \leftarrow \mathrm{X})} \tag{4}$$

here $\varepsilon(\mathrm{A} \leftarrow \mathrm{X})$, $\varepsilon(\mathrm{B} \leftarrow \mathrm{X})$, and $\varepsilon(\mathrm{C} \leftarrow \mathrm{X})$ represent the theoretical partial cross-sections of dissociation channels corresponding to the A, B, and C asymptotic electronic states.

Figure 3 shows the values of β_2 for the angular distributions of Cl(^2P_j, $j = 1/2$) produced from photoexcitation from the vibrational ground level of the X state. It can be seen that the values of β_2 for both Cl($^2P_{1/2}$) are less than zero at wavelengths <330 nm, which is in direct contradiction to the fact that Cl* correlates to the B state, which consists of a parallel transition ($\Delta\Omega = 0$, $\beta_2 = +2$). Considering that the vector properties of the photofragments are usually affected much more by the interactions in the recoupling region than the scalar properties, this finding indicates that the triplet states that affected the asymmetry parameter indeed have effects on the angular distributions of the Cl atom. Thus, other dissociation routes for Cl* must be involved. It can be concluded that the magnitude of the non-adiabatic transition probability p is close to 0.01, which indicates that the coupling strength between the C and 1_u(III) state potentials is prominent. As a consequence, part of the quantum flux will leave the C state and switch to the 1_u(III) state. This suggests that a sufficient amount of the Cl produced by direct excitation from the C state ($\Delta\Omega = 1$, perpendicular transition) is converted to Cl* during dissociation, which adds substantial perpendicular character to the Cl* angular distribution. Over the range 380–470 nm, the p value falls steadily and is virtually equal to zero. Therefore, the coupling strength between the C and 1_u(III) states is negligible, so the wave packet embarked on a C state potential hardly bifurcate in the region where this potential interacts with that of the 1_u(III) state, which makes the C state scarcely able to participate in the angular redistribution of Cl* fragments. Simultaneously, the wave packet propagated on the B state potential evolves solely to Cl* products, which causes Cl* mainly to come from adiabatic dissociation via the B state and only contain parallel transition components. As a result, the β value of Cl* is almost not affected by the dissociation wavelengths and seems to approach the limiting value $\sim +2$ as $\lambda > 380$ nm. Clearly, the angular distribution of the chlorine atom gives a better indication of the effect of the dark states at Franck–Condon transition energies in this case. It is very interesting to note that β_2 values are very different from +2 for the pure parallel transition, and with rapid variations in the short-wavelength region, indicating that the interactions between the two electronic states in the recoupling region may indeed affect the angular distributions of Cl($^2P_j = 1/2$) fragments.

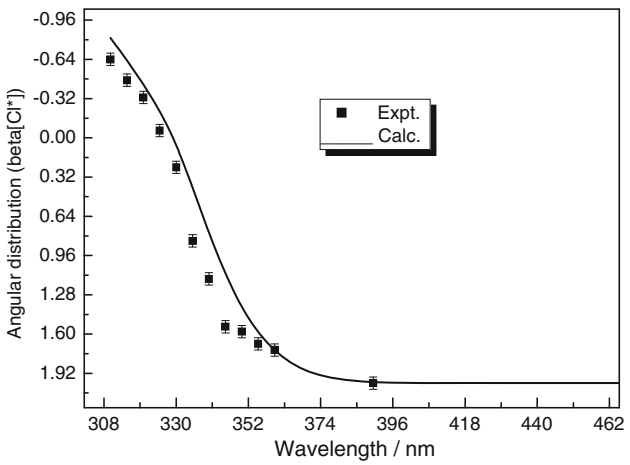

Fig. 3 Wavelength dependence of the calculated angular distribution functions compared with the experimental one (Ref. [21])

Kinetic energy distributions

The momentum distributions $D(k, t)$ of fragments with wave vector k can be obtained by transforming the wave packet $\varphi(r, t)$ from coordinate space into the momentum domain:

$$P(k,t) = |C(p,t)|^2$$

$$D(p,t) = \int \frac{1}{(2\pi\hbar)^{1/2}} \Psi(r,t) \exp(-ikr) dr \tag{5}$$

where $C(p, t)$ is the wave function in the momentum representation. The absorbing potential is removed to keep the

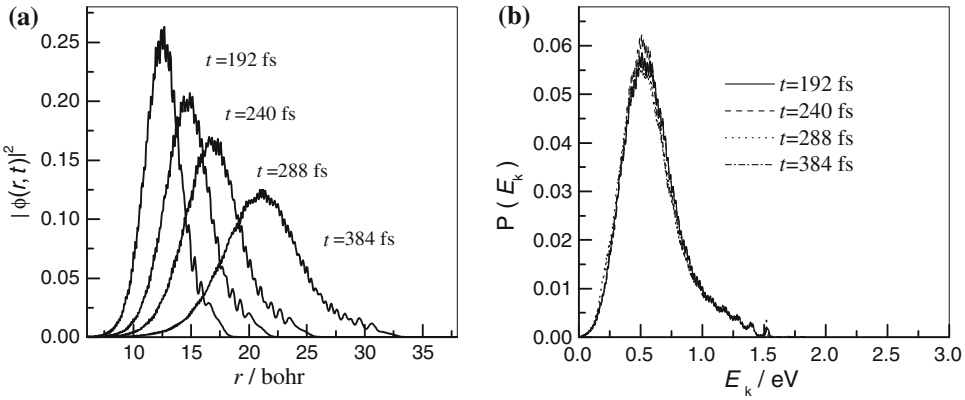

Fig. 4 **a** The squared amplitudes of the wave packets versus internuclear distance; **b** kinetic energy distributions

integrity of $\Psi(r, t)$ perfect. A large grid size is adopted ($r_{max} = 52$ Bohr), which avoids artificial boundary reflection for the time studied.

Figure 4a depicts the probability density functions $|\Psi(r, t)|^2$ at four time instants taken from the snapshots of the wave packet motion along the B state potential of the dissociating Cl_2 molecule. The kinetic energy distributions (KEDs) of fragments, which can be obtained from momentum distributions as $E_k = \hbar^2 k^2/2\mu$, are displayed in Fig. 4b. The threshold of kinetic energy is taken as 3.0 eV, which is equivalent to photon energy. It can be shown that the KEDs change only slightly at different time intervals and converge at 384 fs, by which time the entire wave packet lies on the asymptotic region and dissociation is effectively complete. Without interaction of the covalent bond type, the recoil energy of fragments will be fixed as soon as they come to the asymptotic region. The translational energy E_k is approximately 0.50 eV.

By following the energy conservation principle, $E_{hv} = \Delta E + D_e(X) + E_k$, and substituting the value of the dissociation energy $D_e(X)$ of Cl_2 ($X^1\Sigma_g^+$) at equilibrium, R_e is 2.396 eV, so the fine structure splitting ΔE is concluded to be 838.8 cm^{-1}, which matches the real value of the spin–orbit coupling constant, and serves to validate the excited state potential functions so derived.

Numerical method

The treatments for molecular dissociation dynamics involve solution of the nuclear Schrödinger equation:

$$i\hbar \frac{d}{dt}\left|\Psi(R,t)\right\rangle = \hat{H}\left|\Psi(R,t)\right\rangle \tag{6}$$

where $\hat{H}$ is the time-dependent Hamiltonian and Ψ is the time-developed wavefunction.

The initial wave packets are constructed by multiplying the ground state vibrational wave function $\varphi(R)$ by the appropriate transition moment functions $T(R)$:

$$\begin{pmatrix} \Psi_A(R,t=0) \\ \Psi_B(R,t=0) \\ \Psi_C(R,t=0) \end{pmatrix} = \begin{pmatrix} T_A(R)\cdot\varphi(R) \\ T_B(R)\cdot\varphi(R) \\ T_C(R)\cdot\varphi(R) \end{pmatrix} \tag{7}$$

where $\varphi_j(R, t)$ (j = A, B, and C) denotes the wave packet associated with the specific valence excited state and $T_j(R)$ is the transition moment connecting state j with the ground state.

The wave packet $\Psi(t = 0)$ is propagated on the multiple dissociative surfaces in a series of short time steps. The propagation scheme uses a symmetric splitting operator technique:

$$u(\Delta t) \approx e^{-iV\Delta t/2\hbar} e^{-iT\Delta t/\hbar} e^{-iV\Delta t/2\hbar} + O\left(\Delta t^3\right)$$
$$|\Psi(\Delta t)\rangle = u(t)|\Psi(0)\rangle \tag{8}$$

where Δt is the increment in time and $u(\Delta t)$ is the propagator operator.

The partial cross-section of dissociation for a specific asymptotic channel is obtained by examining the wave packet associated with each excited state potential at an analysis line $R = R_\infty$ in the asymptotic region. The partial cross-section for the jth channel $\varepsilon_j(\omega)$ as a function of excitation frequency ω is extracted by:

$$Q_j(R_\infty, E) = \frac{1}{2\pi}\int_0^\infty \Psi_j(R_\infty, t)\exp\left[i\left(E_{v''} + h\omega\right)t/\hbar\right]dt$$
$$\varepsilon_j(\omega) = \left(\frac{4\pi^3\omega k_j}{3c\varepsilon_0\mu}\right)\left|Q_j(R_\infty, E)\right|^2 \tag{9}$$

where μ is the reduced mass of Cl_2, $E_{v''}$ is the vibrational energy of a given v'' level, and k_j is the wave vector of fragments in channel j, which is deduced from:

$$k_j = \sqrt{2\mu\left(h\omega - V_j(R_\infty)\right)\hbar^{-1}} \tag{10}$$

The calculations are performed using evenly spaced grids for the internuclear coordinate. As reaction flux reaches the asymptotic region, it must be absorbed by an optical potential located in the product channel to avoid an

artificial reflection of the continuum states at the end of the coordinate range under consideration, so the population is gradually dissipated after a long time, which does not give rise to serious problems. Here the negative imaginary potential (NIP) is proposed. The most usual form is a monomial of the power 1.5:

$$V_{NIP}(R,\gamma) = -is_0(\gamma)\left[\frac{R-R_{abs}}{R_{\max}-R_{abs}}\right]^{1.5} \quad \text{for} \quad R_{abs} \le R < R_{\max} \tag{11}$$

where R_{abs} is the starting point of absorption and $s_0(\gamma)$ is chosen in such a way that the sum of reflection and transmission is minimized. In our numerical simulation, we adopt the conditions that the range of the coordinate is $2.83 < R$ (a.u.) < 12.29, the total number of basis grid points is $N = 8{,}192$, and the increment of time coordinate is $\Delta t = 0.24$ fs; $s_0(\gamma)$ and R_∞ are chosen as 0.015 and 8.80 a.u., respectively. The corresponding potential curves relevant to the discussion are calculated at the complete active space self-consistent field level, which is a high-order version of the multiconfigurational self-consistent field (SCF) theory. In the computations, the state-averaged SCF method is used to optimize the relevant molecular orbitals for the averaged state of all configuration derived from (σ_g, π_u, π_g*, σ_u*). The active electrons including valence electrons all come from the 3p atomic orbitals of Cl, and the occupied orbital space is divided into a set of inactive or closed-shell orbitals and a set of active orbitals. The active electrons $N_{\text{act}} = N_{\text{el}} - 2N_{\text{closed}}$ will be distributed in all possible ways among the active orbitals, where N_{closed} is the number of closed-shell (inactive) orbitals, and N_{el} is the total number of electrons. Thus, it corresponds to a full CI in the active space, where the active space consists of ten electrons distributed over six molecular orbitals (MOs), which means all the lone pair orbitals of the chlorine, the bonding orbital $\sigma_{\text{Cl–Cl}}$, and the antibonding orbital $\sigma^*_{\text{Cl–Cl}}$ are considered in the active space. The relativistic ab-initio model potential (AIMP) effective core potentials (ECP) are used for Cl, which are contracted to (5s, 4p, 3d, 2f, 1g).

Conclusion

In this manuscript we investigate theoretically the photodissociation of the Cl_2 molecule in the A-band region. Calculations involving interference effects (RZD formula) are, in principle, essential, because they are expected to contribute substantially to these dissociation processes. Ground and excited electronic states are computed among which the C and the 1_u(III) states, that may allow avoided crossings, are the more relevant ones because of their high transition probability properties. For such transitions, corresponding relevant orbitals (HOMO and LUMO) have been computed. Transition probabilities are calculated as function of the laser wavelengths and for the value of the coupling strength by using the classical RZD theory. The asymmetry term β_2 is estimated from the intensities of the absorption bands in the A, B, and C states with the RZD transition probability. Its wavelength dependence is well reproduced, which shows that the RZD model is appropriate for describing the noncrossing-type transition for homonuclear diatomic molecules with g–u symmetry.

Acknowledgments This work was supported by the Fundamental Research Funds for the Central Universities and Huazhong Agricultural University Scientific and Technological Self-innovation Foundation (2009QC016).

References

1. Duhoo T, Pouilly B (1995) J Chem Phys 103:182
2. DeMille D (2002) Phys Rev Lett 88:67901
3. Tully JC (1980) Adv Chem Phys 42:63
4. Atchity GJ, Xantheas SS, Ruedenberg K (1991) J Chem Phys 95:1862
5. Syage JA, Wessel JA (1988) Appl Spectrosc Rev 24:1
6. Vitanov NV, Garraway BM (1996) Phys Rev A 53:4288
7. Kondorskiy A, Nakamura H (2004) J Chem Phys 120:8937
8. Yang J, Li QS, Zhang SW (2007) Phys Chem Chem Phys 9:466
9. Lindeman TG, Wiesenfeld (1979) J Chem Phys 70:2882
10. Zhang D (2010) Acta Physica Polonica A 117:457
11. Singer SJ, Freed KF, Band YB (1985) Adv Chem Phys 61:1
12. Hall GE, Houston PL (1989) Annu Rev Phys Chem 40:375
13. Dixon RN (1986) J Chem Phys 85:1866
14. Orr-Ewing AJ, Zare RN (1994) Annu Rev Phys Chem 45:315
15. McCaffrey JG, Kunz H, Schwentner N (1992) J Chem Phys 96:2825
16. Li L, Lipert RJ, Lobue J, Chupka WA, Colson SD (1988) Chem Phys Lett 151:335
17. Huang YL, Gordon RJ (1991) J Chem Phys 94:2640
18. Mulliken RS (1930) Phys Rev 36:1440
19. Busch GE, Mahoney RT, Morse RI, Wilson KR (1969) J Chem Phys 51:449
20. Matsumi Y, Kawasaki M, Sato T, Arikawa T (1989) Chem Phys Lett 155:486
21. Matsumi Y, Tonokura K, Kawasaki M (1992) J Chem Phys 97:1065
22. Herberg G (1950) Molecular spectra and molecular structure I, spectra of diatomic molecules. Van Nostrand Reinhold, New York, p 319